Mon. Not. R. Astron. Soc. **000**, 1–12 (—) Printed 10 June 2014 (MN LATEX style file v2.2)

Accretion and Diffusion Timescales in Sheets and Filaments

F. Heitsch[1⋆] and L. Hartmann[2]
[1] *Department of Physics and Astronomy, University of North Carolina Chapel Hill, Chapel Hill, NC 27599-3255, U.S.A*
[2] *Department of Astronomy, University of Michigan, Ann Arbor, MI 48109, U.S.A*

arXiv:1406.2191v1 [astro-ph.GA] 9 Jun 2014

Accepted 2014 June 08. Received 2014 June 08; in original form 2014 March 05

ABSTRACT
A comparison of accretion and (turbulent) magnetic diffusion timescales for sheets and filaments demonstrates that dense star-forming clouds generally will – under realistic conditions – become supercritical due to mass accretion on timescales at least an order of magnitude shorter than ambipolar and/or turbulent diffusion timescales. Thus, ambipolar or turbulent diffusion – while present – is unlikely to control the formation of cores and stars.

Key words: methods: analytical—stars: formation—ISM: clouds—gravitation—MHD

1 INTRODUCTION

The role of magnetic fields in star formation has been debated for many decades. Mestel & Spitzer (1956) showed that spherical or isotropic contraction from conditions in the diffuse interestellar medium would prevent gravitationally-bound solar-mass protostellar clouds from forming unless substantial amounts of magnetic flux were lost during contraction. They suggested that this flux loss was a result of ambipolar diffusion in dark clouds where the ion fraction becomes very low due to dust shielding of the interstellar radiation field. Following this work, a large number of investigations have been dedicated over the years to examining the effects of magnetic fields on the rotation and structure of protostellar clouds and their time evolution (Mouschovias 1979a,b; Ciolek & Mouschovias 1993; Ciolek & Basu 2000, 2006, see also Shu et al. 1987).

In its most extreme form, the picture of protostellar cloud contraction controlled by ambipolar diffusion led to the concept of "slow" star formation (Shu et al. 1987). The lengthy diffusion timescales in principle would then explain the low efficiencies of star formation in molecular clouds (Cohen & Kuhi 1979; Evans et al. 2009). However, studies of the stellar populations in molecular clouds show that the stars are generally young - a few Myr old at most - , and they show no evidence for substantial numbers of older ($\sim$ 10 Myr-old) stars. This has led to the countervailing picture of "rapid" star formation (Hartmann et al. 2001), in which ambipolar diffusion does not play a major role in lengthening collapse timescales. In this picture the efficiency of star formation is not determined by slow contraction but rather by cloud dispersal via stellar energy input (Franco et al. 1994; Dale et al. 2005; Walch et al. 2012)[1], or possibly by tidal forces for lower-mass clouds (Ballesteros-Paredes et al. 2009a,b).

A mechanism which might reduce the timescale for the diffusion of magnetic flux is turbulence. This possibility has been explored in the context of turbulent ambipolar diffusion (Zweibel 2002; Kim & Diamond 2002; Fatuzzo & Adams 2002; Heitsch et al. 2004; Li & Nakamura 2004; Kudoh & Basu 2008, 2011), and of reconnection diffusion (Lazarian & Vishniac 1999; Santos-Lima et al. 2010; Eyink et al. 2011, 2013).

Alternatively, Mestel & Spitzer (1956) recognized that the "magnetic flux problem" could be avoided by mass accumulation along field lines, which could achieve the necessary mass-to-magnetic flux ratio without reducing the magnetic flux. They rejected this solution, however, by arguing that the mass would have to be accumulated over such long length scales that it would gravitationally fragment. We now understand that this argument is not applicable because the interstellar medium is generally in supersonic motion, and the usual Jeans criterion based on balancing thermal pressure against gravity is irrelevant. Indeed, numerical simulations of the large-scale galactic interstellar medium show precisely this accumulation of mass along field

⋆ E-mail: fheitsch@unc.edu (FH); lhartm@umich.edu (LH)

[1] Walch et al. (2012) point out that the role of stellar feedback depends on the cloud mass (Dale et al. 2012). Also, once the cloud is allowed to continue to accrete material during the feedback phase, feedback not necessarily disperses the cloud, but keeps gas from reaching the high densities necessary for star formation (Vázquez-Semadeni et al. 2010).

lines (Vázquez-Semadeni et al. 1995; Hartmann et al. 2001, see also Kim & Ostriker 2006).

Support for the idea of mass accumulation along field lines comes from the comprehensive observational analysis of Crutcher et al. (2010), who found no evidence for increasing average field strength with increasing density below $n \sim 300$ cm^{-3} (see also Troland & Heiles 1986, but Marchwinski, Pavel, & Clemens 2012 for newer results from polarimetry). At higher densities, the maximum field strength increases as $B \propto n^{2/3}$, which Crutcher et al. suggest is due to isotropic contraction under gravity. In addition, recent studies of star formation occurring in filamentary gas structures, which appears to be common (André et al. 2010), also provide support for the idea of building dense structures initially via flows along the magnetic field. In some well-studied cases, such as B216/17, B18, L1506 (Heyer et al. 1987; Goodman et al. 1990; Moneti et al. 1984) and B211/13 in Taurus (Palmeirim et al. 2013), and the Pipe Nebula (Alves et al. 2008) the magnetic field appears relatively ordered and nearly perpendicular to the filamentary gas, as would be expected in this scenario. Furthermore, Palmeirim et al. (2013) show that the CO emission around B211 exhibits differing radial velocities on either side of the filament, interpreting this as evidence for inflow of ambient molecular gas. For a systematic study of the alignment of ambient magnetic fields with local molecular clouds, see Li et al. (2013).

These observational results motivate us to address the question of ambipolar and turbulent diffusion vs. mass accumulation using a relatively simple geometric setup. We compare the accretion and diffusion timescales for magnetized sheets (Sec. 2) and filaments (Sec. 3), based on an earlier study discussing the evolution of the Pipe nebula (Heitsch et al. 2009). We find for both sheet- and filament-like geometries that accretion will dominate a cloud's evolution from subcritical to supercritical.

2 ACCRETION AND AMBIPOLAR/TURBULENT DIFFUSION TIMESCALES FOR A SHEET

We assume that star-forming molecular clouds are assembled by flows along magnetic field lines. This is reasonable given the fact (a) that perpendicular field components can efficiently prevent compression and high density contrasts (Inoue & Inutsuka 2008, 2009; Heitsch et al. 2009), and (b) that magnetic field vectors seem aligned perpendicularly to filamentary structures (Heyer et al. 1987; Palmeirim et al. 2013, see also Hartmann (2002) for a scenario). We envision cloud formation to occur conceptually in two phases. The first involves the accumulation of lower-density gas as a result of large-scale flows in the interstellar medium (Sec. 2.1). This has usually been considered in terms of the sweep-up of diffuse atomic gas (Vázquez-Semadeni et al. 1995; Hartmann et al. 2001), though there is no reason why, in environments other than the solar neighborhood, accumulation of partially or mostly diffuse molecular gas cannot occur as well (Pety et al. 2013). The second phase addresses the observation that star formation occurs in the densest regions of molecular clouds, where such regions generally represent a small fraction of the total cloud mass (Lada et al. 2010; Heiderman et al. 2010). We explore this later phase (Sec. 2.2) by considering the development of denser sheets and filaments within the molecular cloud driven by self-gravity (e.g. Vázquez-Semadeni et al. 2007).

2.1 Cloud Formation by Sweep-up of Diffuse Gas

We assume that the cloud is forming due to the collision of two identical flows of diffuse atomic gas, with constant density n_0 and velocity v_0. The flows are parallel to the background magnetic field B. Then, the cloud can be treated as a "sheet" of column density N_H, accreting gas at a rate $2n_0v_0$, or

$$\begin{aligned} N_H &= 2n_0v_0t \qquad (1)\\ &= 6.31\times10^{20}\left(\frac{n_0}{\mathrm{cm}^{-3}}\right)\left(\frac{v_0}{10\mathrm{km\ s}^{-1}}\right)\left(\frac{t}{\mathrm{Myr}}\right)\ \mathrm{cm}^{-2}. \end{aligned}$$

A thin sheet that is permeated by a magnetic field B can fragment if

$$N_H > \frac{B}{2\pi m G^{1/2}}, \qquad (2)$$

or, if the mass-to-flux ratio at a given mass column density $\Sigma = mN_H$ is larger than the critical value,

$$\frac{\Sigma}{B} > \left(\frac{\Sigma}{B}\right)_c \equiv \frac{1}{2\pi G^{1/2}}, \qquad (3)$$

(Nakano & Nakamura 1978). The time τ_{acc} needed for the cloud to reach criticality results from equations 1 and 2,

$$\begin{aligned} \tau_{acc} &= \frac{B}{4\pi n_0 v_0 m G^{1/2}} \qquad (4)\\ &= 5.65\left(\frac{B}{5\mu\mathrm{G}}\right)\left(\frac{n_0}{\mathrm{cm}^{-3}}\right)^{-1}\left(\frac{v_0}{10\mathrm{km\ s}^{-1}}\right)^{-1}\ \mathrm{Myr}. \end{aligned}$$

The ambipolar diffusion timescale at a given length scale L can be written as (see App. A)

$$\tau_{AD} = 1.38\times10^3\left(\frac{L}{\mathrm{pc}}\right)^2\left(\frac{n}{3\times10^2\mathrm{cm}^{-3}}\right)^{3/2}\left(\frac{B}{5\mu\mathrm{G}}\right)^{-2}\ \mathrm{Myr}. \qquad (5)$$

Note that we use a different scaling for the density corresponding to the transition from $B \propto n^0$ to $B \propto n^{2/3}$ (Crutcher et al. 2010), since we are interested in ambipolar diffusion *within* the sheet-like cloud. Comparing equations 4 and 5 suggests that accretion may be faster than ambipolar diffusion on the whole.

More specifically, we discuss two regimes. (1) For a cloud forming from the diffuse interstellar gas via sweep-up, we set the flow densities and velocities to 1 cm^{-3} and 10 km s^{-1}. For the (still) diffuse, forming cloud, we assume $n = 300$ cm^{-3}, and a length scale of a parsec. For these numbers, accretion is faster than ambipolar diffusion ($\tau_{acc} < \tau_{AD}$) if $B \lesssim 30\mu$G. Note that ambipolar diffusion will not be relevant before a (UV-shielding) column density corresponding to $A_V = 1$ (or $B \approx 8\mu$G) has been accumulated (see App. A). (2) Once sufficient mass has been accumulated, the accretion flows will start to be driven by gravity (see Sec. 2.2). In this case, we assume a flow density of 100 cm^{-3}, and a flow velocity of 1 km s^{-1}. At the same lengthscale of 1 pc, $\tau_{acc} < \tau_{AD}$ for $B \lesssim 540\mu$G. At a tenth of a parsec, the condition is reached for $B \lesssim 5.4\mu$G.

2.2 Dense Gas Formation by Gravitationally Driven Flows

We next follow the evolution of a sheet-like cloud that is allowed to accrete gas at free-fall velocities. Here we are thinking of the accumulation of diffuse molecular gas - usually constituting the majority of the cloud - driven by gravity into a dense structure that can form stars, adopting a sheet geometry for simplicity (we consider filaments in Sec. 3). The gravitational acceleration towards an infinite sheet with mass column density Σ is given by

$$|a_s| = 2\pi G\Sigma\,. \tag{6}$$

For steady-state accretion, the velocity profile can be written as

$$v_z = -2(\pi G\Sigma(z_{ref} - z))^{1/2}, \tag{7}$$

if we assume that Σ does not vary strongly while the column of ambient gas

$$\Sigma_{acc} \equiv 2\rho_0 z_{ref} \tag{8}$$

is accreted. We will justify this assumption in Appendix B. Here, z_{ref} is a reference distance to be chosen, and will be on the order of 1 pc. For a field strength of 10μG (using eq. 2), this results in an infall velocity of 1 km s^{-1}, consistent with observational estimates (Kirk et al. 2013; Friesen et al. 2013; Palmeirim et al. 2013).

We ignore the ram pressure of the infalling gas (see App. C). Thus, we can set z in equation 7 to the scaleheight of an isothermal sheet (at given sound speed c_s),

$$H = \frac{c_s^2}{\pi G\Sigma}. \tag{9}$$

Then, the accretion rate onto the sheet is given by

$$\begin{aligned}\dot{\Sigma} &= 2\rho_0 v_z \\ &= 4\rho_0\left(\pi G z_{ref}\Sigma\left(1-\frac{H}{z_{ref}}\right)\right)^{1/2} \\ &= a\left(\Sigma - b\right)^{1/2}. \end{aligned} \tag{10}$$

In the last step we defined

$$a \equiv 4\rho_0\left(\pi G z_{ref}\right)^{1/2} \tag{11}$$

$$b \equiv \frac{H}{z_{ref}}\Sigma = \frac{c_s^2}{\pi G z_{ref}}. \tag{12}$$

The solution to eq. 10 is

$$\Sigma(t) = \frac{1}{4}\left(a^2t^2 + 2a\Sigma_0^{1/2}t + 4b + \Sigma_0\right), \tag{13}$$

with the initial column density $\Sigma_0 = mN(t=0)$ to be chosen. Equating this with eq. 2 and solving for the accretion time τ_{acc} yields

$$\tau_{acc} = \frac{1}{a}\left(2\left(\frac{B}{2\pi G^{1/2}} - b\right)^{1/2} - \Sigma_0^{1/2}\right). \tag{14}$$

To develop physical insight, we further simplify equation 14. First, we can choose Σ_0, the initial column density, to be negligibly small, i.e. $\Sigma_0 \ll \Sigma_c \equiv B/(2\pi\sqrt{G})$. Second, b is essentially the ratio of H/z_{ref}, which for an evolved sheet will also be small, if we set $z_{ref} = 3$ pc. With these simplifications, equation 14 turns into

$$\tau_{acc} \approx \left(2\pi G\rho_0\right)^{-1/2}\left(\frac{\Sigma_c}{\Sigma_{acc}}\right)^{1/2}, \tag{15}$$

i.e. the timescale to reach criticality is given by the free-fall time of the ambient gas multiplied by the square root of how many columns of Σ_{acc} are needed to achieve criticality. The criticality parameter $\mu(t)$ can be derived directly from eq. 13, as can the ambipolar diffusion timescale τ_{AD}, using the fact that $\Sigma = 2\rho_c H$.

2.3 Comparison of Timescales

Figure 1 summarizes the evolution of an infinite, magnetized sheet accreting diffuse molecular gas via gravity (Sec. 2.2). The ambient gas density is $n_0 = 100$ cm^{-3}, and the reference distance $z_{ref} = 3$ pc. The criticality parameter (panel (a)) is proportional to the column density. Vertical lines indicate τ_{acc} (eq. 14). Comparing τ_{acc} to the ambipolar diffusion timescale (panel (b), solid lines labeled τ_{lam}), we see that $\tau_{acc} \ll \tau_{lam}$. Figure 1 of Crutcher et al. (2010) suggests that for densities $10^3 < n < 10^4$ cm^{-3}, the upper limit for the field strength is between 30 and 100μG. Yet, such densities would not be expected at early evolutionary stages (which are of concern here), thus, we do not consider magnetizations higher than 30μG. It is easy to see that cranking up the magnetic field strength would eventually lead to a regime where $\tau_{lam} < \tau_{acc}$, but such a regime is not physically accessible. Finally, it is worth pointing out that for $t = 0$, there would be no sheet. The cloud would appear in CO when an $A_V \approx 1$ is reached. For typical flow parameters, this occurs a few Myr after flow collision (Heitsch & Hartmann 2008).

The physically correct length scale for laminar ambipolar diffusion would be the gravitational forcing scale, i.e. the fastest-growing, gravitationally unstable mode λ_{max} of a magnetized sheet (Larson 1985, see panel(c), long-dashed lines). Note that while we show λ_{max}, the growth rate drops only slowly for wavelengths $\lambda > \lambda_{max}$. For instance, at $\lambda = 5\lambda_{max}$, the timescale is only $\sim 60\%$ longer than at λ_{max}. Thus, we slightly underestimate the relevance of fragmentation in Figure 1. Since this length scale is undefined for $\mu \leq 1$, we also show the corresponding hydrodynamical scale (Larson 1985, long-dashed lines in panel (c)). The short-dashed line shows the scaleheight H (eq. 9) for comparison. The latter would be an inappropriate choice for an ambipolar diffusion scale in this context, since we are not interested in the *vertical* diffusion of the magnetic field. Summarizing, *the sheet turns supercritical due to accretion on timescales substantially shorter than the laminar ambipolar diffusion timescale.*

Can turbulence accelerate ambipolar diffusion sufficiently to win over accretion? While there is a variety of implementations of turbulent ambipolar diffusion, such as acceleration through stagnation point flows (Zweibel 2002), stochastic acceleration through field and density variations (Fatuzzo & Adams 2002), turbulent mixing generating small scales (Heitsch et al. 2004) and – to a large extent combining much of the above – turbulent compression (Li & Nakamura 2004), they all sugest that turbulent ambipolar diffusion can break the flux-freezing assumption on dynamical rather than on diffusive timescales. While we will focus our discussion on turbulent *ambipolar* diffusion for the sake of consistency with previous literature (Li & Nakamura 2004; Kudoh & Basu 2011), the exact mechanism of how flux-freezing is broken at the smallest scales may not be that relevant, as long as the turbulent diffusivity $\lambda_{trb} \gg \lambda_{lam}$, the

laminar diffusivity (e.g. Kim & Diamond 2002, see, however, Santos-Lima et al. 2010 for a different point of view). Thus, λ_{lam} could also be due to Ohmic dissipation. Numerical evidence for reconnection diffusion (Lazarian & Vishniac 1999) is given by Eyink et al. (2013). Thus we will speak of *turbulent diffusion* in the following, with the understanding that $\lambda_{lam} = \lambda_{AD}$ (see eq. A4) in our calculations.

The short-dashed curves in panel (b) of Figure 1 trace the evolution of

$$\tau_{trb} = \frac{H^2}{\lambda_{AD} + H\sigma}. \tag{16}$$

Here we argue that the ambipolar "diffusivity" λ_{AD} (eq. A4) is enhanced by a turbulent diffusivity of $\lambda_{trb} = \sigma H$, where H is chosen as an outer turbulent scale assuming isotropic turbulence, and σ is the turbulent *rms* velocity. For the latter, we assume that turbulence within the sheet can be driven by accretion (Klessen & Hennebelle 2010), and can be written as

$$\begin{aligned} \sigma &= \left(4\epsilon\, H\, v_z(H)^2 \dot{\Sigma}/\Sigma\right)^{1/3} \qquad (17)\\ &= (4\epsilon)^{1/3} v_z(H) \\ &= 0.74 \left(\frac{\epsilon}{0.1}\right)^{1/3} \left(\frac{N}{10^{21}\ \mathrm{cm}^{-2}}\right)^{1/2} \left(\frac{z_{ref}}{\mathrm{pc}}\right)^{1/2} \mathrm{km\ s}^{-1}, \end{aligned}$$

with a driving efficiency $\epsilon = 0.1$ (see Heitsch 2013a, for a discussion based on Klessen & Hennebelle 2010). With equations 17 and 9, the turbulent diffusivity reads

$$\lambda_{trb} = 3.6{\times}10^{22} \left(\frac{\epsilon}{0.1}\right)^{1/3} \left(\frac{N}{10^{21}\ \mathrm{cm}^{-2}}\right)^{-1/2} \left(\frac{z_{ref}}{\mathrm{pc}}\right)^{1/2} \mathrm{cm^2\ s^{-1}}. \tag{18}$$

The scaleheight H is on the order of a tenth to a few tenths of a parsec. Comparing the turbulent diffusivity λ_{trb} to the laminar ambipolar diffusivity λ_{AD} (eq. A4), we see that for conditions as to be found in molecular clouds, $\lambda_{trb} \gg \lambda_{AD}$.

From Figure 1 we see that although orders of magnitude shorter than the laminar ambipolar diffusion timescale τ_{lam}, $\tau_{trb} < \tau_{acc}$ only for the strongest magnetization, which, however is irrelevant at early times. Also, though $\tau_{trb} > \tau_{max}$ for ~ 0.5 Myr directly after the sheet turns supercritical, this timespan is much shorter than τ_{trb} at that point[2]. *Thus, we conclude that turbulent diffusion does not dominate the criticality of the sheet.*

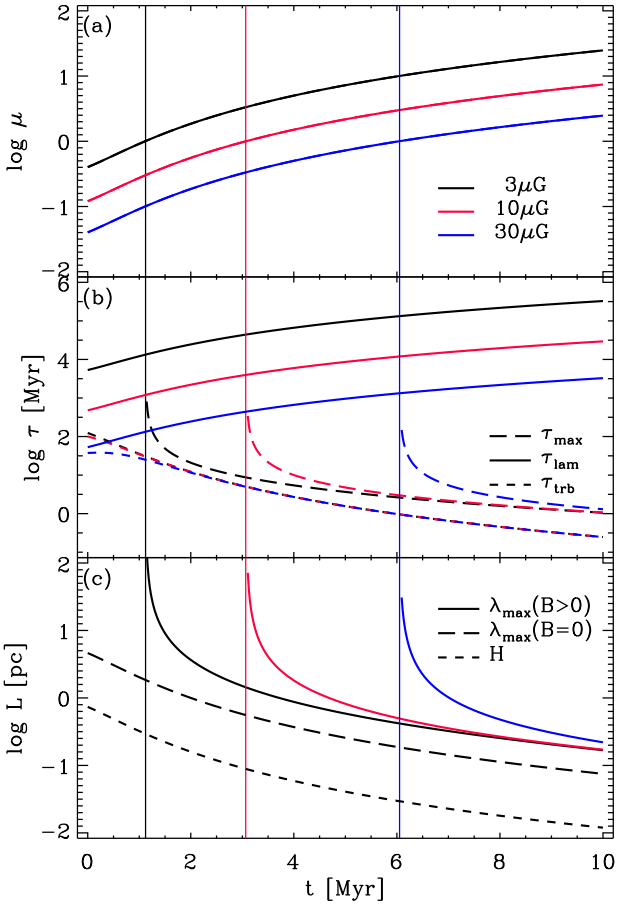

Figure 1. Time evolution of a sheet accreting at free-fall velocities. (a) Magnetic criticality parameter μ (from eqs. 2, 13) for magnetic field strengths $[3, 10, 30]\mu$G as indicated. Vertical lines denote the time τ_{acc} (eq. 14) at which $\mu = 1$. (b) Fastest-growing gravitational mode τ_{max} of a magnetized sheet (long-dashed lines), laminar ambipolar diffusion timescale τ_{lam} (eq. 5, solid lines), and turbulent diffusion timescale (eq. 16, short dashed lines). The sheet can become supercritical solely due to accretion on time scales (substantially) shorter than the ambipolar diffusion timescales. (c) Fastest-growing gravitational length scale λ_{max} of a magnetized sheet (solid lines, Larson 1985), fastest-growing gravitational mode for an unmagnetized sheet (Larson 1985, long-dashed lines), and scaleheight H (eq. 9, short dashed lines). The background density is set to $n = 100$ cm^{-3}, and the reference distance to $z_{ref} = 3$ pc.

3 ACCRETION AND AMBIPOLAR/TURBULENT DIFFUSION TIMESCALES FOR A FILAMENT

While for the accreting sheet the choice of field orientation is fairly obvious, and results in $B \propto \rho^0$, the situation for an accreting filament is less so. Motivated by observational constraints (see Sec. 1), we assume a planar field geometry, with the field perpendicular to the filament. Thus, material is free to flow (mostly) within the field plane onto the filament. Such a geometry would result in $B \propto \rho^0$, and an accretion rate of $\sim 4\rho_0 v_0 H$, where H is the scaleheight of the filament. It may be less restrictive to assume that the inflow is not restricted to the plane, but extends over the whole azimuthal range. If mass and flux are conserved during radial contraction, then $B \propto \rho^{1/2}$, a scaling that is also more consistent with the observed increase in field strength at higher densities (Crutcher et al. 2010).

[2] The referee points out that the horizontal diffusion timescale may not be the most important one, for two reasons. First, compression without a horizontal component would leave the field unaffected, and thus horizontal diffusion would be irrelevant. Yet, this applies only to infall of gas of uniform density. Overdensities could lead to local enhancements, and thus horizontal perturbations. Second, if there is horizontal compression, the bent field lines would attempt to straighten, leading to horizontal diffusion. This is briefly discussed in App E.

3.1 Model

We follow the evolution of a filament under free-fall, steady-state accretion, using a model series of externally pressurized, accreting cylinders, with $B \propto \rho^{1/2}$ (Heitsch 2013b). Assumptions, derivations and expressions can be found in that paper. Since we envisage the filaments to be embedded in a flattened, evolved molecular cloud, we set the ambient density to 100 cm^{-3}, corresponding to diffuse molecular gas. Infall velocities range around a km s^{-1} (see Fig. 1 of Heitsch 2013b). We calculate two criticality parameters: The radial criticality parameter

$$\mu_{rad} \equiv \frac{m}{m_{rad}} \tag{19}$$

compares the filament's line mass m with the critical magnetic line mass,

$$m_{rad} = 0.24\frac{BR}{\sqrt{G}} + 1.66\frac{c_s^2}{G}, \tag{20}$$

as determined numerically by Tomisaka (2013). For the longitudinal criticality parameter, we adapt the expressions given by Bastien (1983) for the number of Jeans masses in a magnetized, prolate ellipsoid with axes $a > b = c$,

$$\mu_{lon} \equiv \frac{\pi G\rho c^2}{15ec_s^2}\ln\left(\frac{1+e}{1-e}\right), \tag{21}$$

where the ellipticity e is defined by $c^2 = a^2(1-e^2)$. We use an aspect ratio of $a/c = 10$. Larger aspect ratios increase μ_{lon}, thus, we can consider our choice as a lower bound. As Bastien (1983) discusses, the limit towards high ellipticity (infinitely long filaments) yields an infinite Jeans number and thus does not converge to the radial expression, since these are different collapse modes. Ambipolar diffusion timescales are calculated as above. The wavelength of the fastest-growing mode depends on whether the filament resides in a vacuum (infinite radial extent, or an infinite overpressure, Ostriker 1964), or whether a "truncated" (or pressurized, Fischera & Martin 2012a) filament is considered. We show both cases for comparison, using the expressions given by Nagasawa (1987) for the infinite cylinder, and the polynomial fits by (Fischera & Martin 2012a) for the pressurized cylinder. For the sake of simplicity, we forego the discussion of varying external pressure due to accretion (Heitsch 2013b).

3.2 Comparison of Timescales

Figure 2 summarizes the evolution of a filament accreting at free-fall velocities, assuming $B \propto \rho^{1/2}$. Results are shown for two magnetizations, corresponding to *initial* field strengths of 2 and 6μG. During the evolution of the filament, fields $\gtrsim 100\mu$G are reached (see also Sec. 4).

Evolution timecales are below one Myr overall. The filaments reach criticality after a fraction of a Myr (panel (a)), with global longitudinal criticality μ_{lon} (eq. 21) close to radial criticality μ_{rad} (eq. 19), and winning for weak magnetizations. Panel (b) shows that the fragmentation timescales drop to values close to the longitudinal accretion timescale. The laminar (τ_{lam}, solid lines) and turbulent diffusion timescales (τ_{trb}, dashed lines) are all longer than the time to reach (longitudinal) criticality, and they are all larger than 10 Myr at τ_{acc}, although they do drop for times $> \tau_{acc}$. Yet that drop is irrelevant for our purposes: the filament already has grown critical due to accretion. *Thus, as in the sheet case, filaments are likely to reach criticality through accretion, before ambipolar diffusion can have a significant effect.* Note that the timescales in panel (b) refer to externally pressurized (truncated) cylinders (Fischera & Martin 2012b). The corresponding timescales for cylinders in vacuum (Ostriker 1964; Nagasawa 1987) differ only for small evolution times, being always larger than for truncated cylinders (only shown in Fig. 2 for the length scales). Panel (c) shows the length scales of the fastest growing mode, derived for infinite (Nagasawa 1987, solid lines) and pressurized (Fischera & Martin 2012a, dashed lines). As the latter authors discuss, the expressions converge for large line masses, i.e. larger overpressures.

4 DISCUSSION

We compared ambipolar diffusion and accretion timescales for sheets (Sec. 2) and filaments (Sec. 3), finding that in both geometries, accretion will dominate the evolution from sub- to supercritical structures. For the sheets, we considered two cases; the assembly of a molecular cloud from the diffuse (atomic) interstellar medium, and the evolution of a dense cloud due to accretion of ambient molecular gas. For the filament geometry, we only consider gravitationally driven accretion.

Our assumption of free-fall accretion may seem overly extreme. Yet, already order-of magnitude estimates (eqs. 4, 5) with constant (rather low) velocities suggest that accretion dominates over ambipolar diffusion. Also, accretion velocities are at most on the order of a km s^{-1} (Heitsch 2013a,b), consistent with observed values (Kirk et al. 2013; Friesen et al. 2013).

4.1 Sheets

4.1.1 Choice of Length Scales

The choice of length scales is somewhat open, yet not completely arbitrary. We are interested in motions perpendicular to the magnetic field. The only characteristic length available in the sheet plane is that of the gravitationally most unstable mode (this also would be the length scale at which the strongest forces occur). Shorter length scales will not be unstable yet, and longer scales would grow more slowly. One could argue that substructure in the sheet could reduce the length scale, and thus the laminar ambipolar diffusion timescale. Yet (1) the substructure would have to be non-linear, specifically in a finite sheet, to win over large-scale collapse modes (Burkert & Hartmann 2004; Pon et al. 2012), and (2) this case is addressed by the turbulent diffusion timescale. Note that for the latter, the "forcing scale" is still set by the gravitationally most unstable mode. Such an interpretation is also consistent with the findings of Heitsch et al. (2004), that turbulent ambipolar diffusion is not a flux transport mechanism, but acts through breaking the flux-freezing assumption locally.

Since the choice of length scales may be contentious (and is relevant for the interpretation of our results), we highlight its role in Figures 3 and 4. They map out the

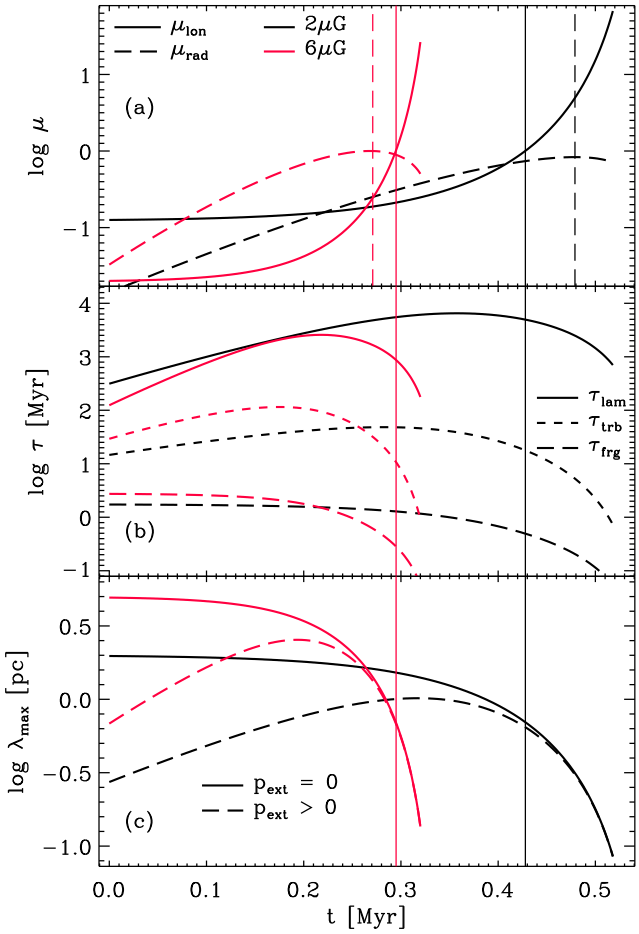

Figure 2. Time evolution of a filament accreting at free-fall velocities. (a) Longitudinal (solid lines, eq. 21) and radial (dashed lines, eq. 19) criticality parameters. Longitudinal and radial criticality (indicated by vertical lines) are reached at about the same time, with longitudinal criticality winning over radial for weak magnetizations. Thus, material will collect first *along* the filament. (b) Laminar ambipolar diffusion timescale (solid lines), turbulent diffusion timescale (dashed lines), for length scales set by the gravitationally most unstable mode (panel (c)). Fragmentation timescales (long-dashed lines) are substantially shorter than ambipolar diffusion timescales at time criticality is reached. (c) Length scales of gravitationally most unstable mode. We distinguish between infinite (solid lines) and finite (dashed lines) cylinders. They converge for large line masses, or large overpressures (Fischera & Martin 2012a).

regimes of the shortest (dominant) timescale in the length-density plane ($\log L, \log n$). Colors stand for timescales, indicated by *acc* for accretion (blue), *frg* for fragmentation (red), *lam* for laminar ambipolar diffusion (light green), and (for Fig. 4) *trb* for turbulent diffusion (dark green). The fragmentation timescale (Larson 1985, see Sec. 2.3) varies following the full dispersion relation. The turbulent diffusion timescale is calculated using the length scale on the x-axis. We chose to present two versions of these maps, one (Fig. 3) without, and the other with turbulent diffusion (Fig. 4). Each Figure contains maps for six magnetic field strengths ($6, 20, 40, 60, 80, 100\mu$G). In each map, the solid line traces the gravitationally most unstable mode derived from Larson (1985, see Appendix D), and the short dashed line stands for the scaleheight of the sheet (eq. 9). Criticality is indicated by the horizontal, long-dashed line, combining equations 2 and 9, and the expressions for the central density in an isothermal sheet, $\rho_0 = \Sigma/(2H)$, to

$$\rho_{crit} = \frac{B^2}{8\pi c_s^2}. \tag{22}$$

In other words, the critical central density is given by comparing the magnetic and thermal pressure, under the assumption that the field is perpendicular to the disk.

Figures 3 and 4 can be used in various ways. First, we can ask for which combinations of length scale and central density ambipolar diffusion might be relevant. This alleviates the problem of having to fix the length scale in our earlier discussion. Second, one can easily read off an evolutionary sequence (via the density-scaleheight relation, eq. 9) from a subcritical to a critical state for a given field strength, and check whether the sheet gets supercritical due to accretion before reaching the ambipolar diffusion regime (laminar or turbulent). It is worth pointing out that the indicated field strength refers to the diffuse ISM, *if* the lines for $H(n)$ and $\lambda_{max}(n)$ are interpreted as evolutionary sequences, since under our assumption $B \propto \rho^0$. The density of the inflows is kept constant at $n = 100$ cm^{-3}.

4.1.2 Model Comparison

In a series of papers, Kudoh & Basu (2008, 2009, 2011) explored the gravitational fragmentation of infinite, magnetized, sheet-like clouds mediated by ambipolar diffusion. In their most recent work, they find that laminar ambipolar diffusion results in a fragmentation timescale of a few 10^7 years, while the presence of moderately supersonic flows can reduce the fragmentation timescale by a factor of 10. Ballesteros-Paredes & Hartmann (2007) discuss that the former timescale is inconsistent with local observations of stellar age spreads of young stars in molecular clouds. Yet, leaving that issue aside for the moment, we attempt to put the results of Kudoh & Basu in the context of our timescale discussion.

Kudoh & Basu (2011) quote characteristic values (assuming a sound speed and a density) for their models. Specifically, at a sound speed of 0.2 km s^{-1}, identical to what we use in our discussion, and a central sheet density of $n = 10^4$ cm^{-3}, their choice of $\beta = 1.0$ results in a field strength of $B = 20\mu$G, and that of $\beta = 0.25$ in $B = 40\mu$G (this would correspond to their model V2). We indicate two length scales in the corresponding panels ($20, 40\mu$G) of Figures 3 and 4 by white diamonds: The smaller length scale is the scaleheight of the sheet, and the larger length scale is the scale of the largest turbulent mode in their simulation.

A glance at Figure 3 (for $B = 20, 40\mu$G) highlights the situation for laminar ambipolar diffusion: even at a scale corresponding to the scaleheight of the sheet (0.05 pc for the parameters above), $\tau_{acc} < \tau_{AD}$, and thus, the sheet will become critical due to accretion before ambipolar diffusion can have a significant effect. Following the dashed line (i.e. the scale height in dependence of density) towards lower densities can be used as a (reverse) evolutionary sequence for a mass-accreting sheet (and thus increasing Σ and ρ). For $B = 40\mu$G, only sheets with central densities $\lesssim 10^3$ cm^{-3}

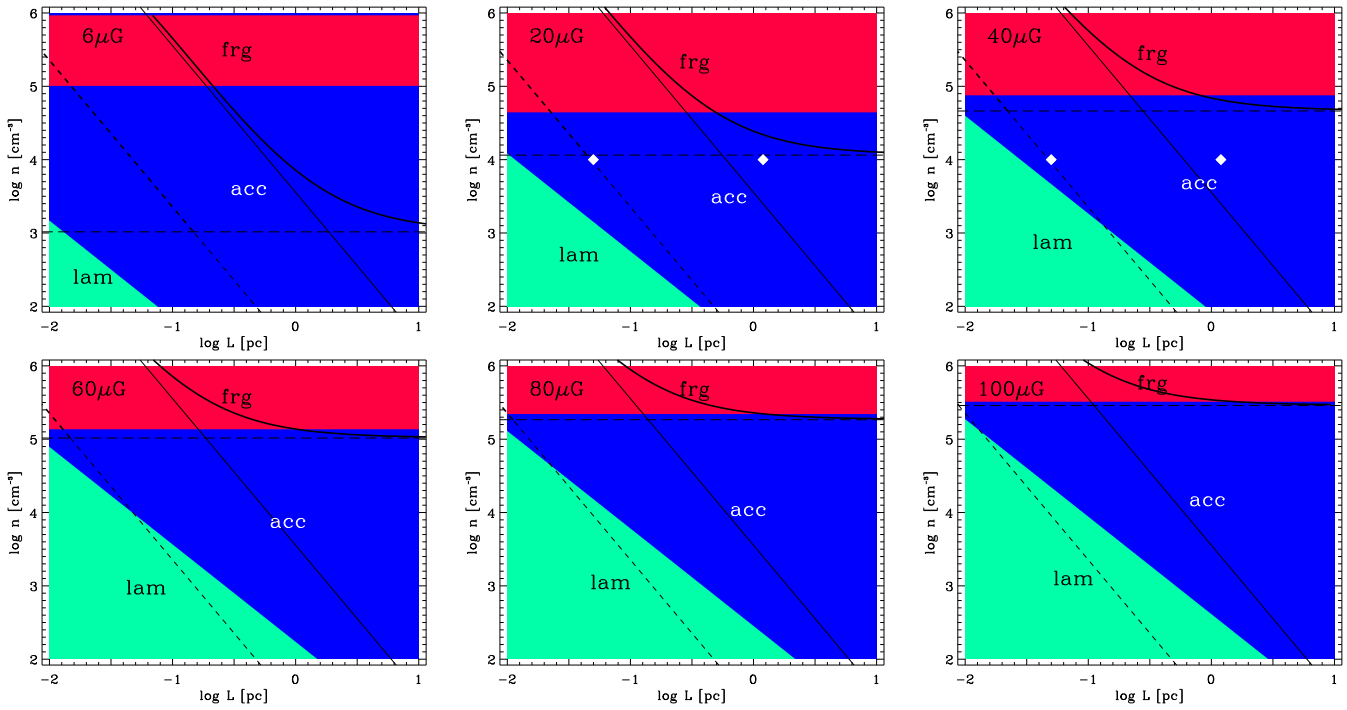

Figure 3. Map of the shortest timescales in the length scale-density plane for a sheet. For a given combination of (L, n), all relevant timescales are compared, and the regime of the shortest timescale is color-coded as blue for accretion (*acc*), red for gravitational fragmentation (*frg*), and light green for laminar ambipolar diffusion (*lam*). The solid curved line shows the wavelength of the most unstable (magnetized) mode, λ_{max}, against the sheet's central density (Larson 1985), the solid straight line is the corresponding hydrodynamical mode, and the dashed line shows the sheet's scaleheight against central density. Criticality is indicated by the horizontal, long-dashed line (eq. 22). White diamonds show the initial conditions for models run by Kudoh & Basu (2011, see Sec.4.1.2).

are dominated by ambipolar diffusion on scales of H. For larger scales, accretion still wins. For $B = 20\mu$G, there is no viable range of densities for ambipolar diffusion to be dominant.

Turbulent diffusion (Fig. 4) will dominate over accretion on length scales of the scale height H at 20 and 40μG (and for any higher magnetization), yet, the scale of the fastest growing mode as well as the outer turbulent scale of the simulations by Kudoh & Basu (2011) are still residing in the accretion-dominated (blue) regime. It should be noted that the "turbulent diffusion" discussed here assumes a different mechanism than the ambipolar diffusion acceleration in Kudoh & Basu's work. Here, we assume that the laminar ambipolar diffusion rate can be accelerated by a turbulent diffusivity (see, e.g., Kim & Diamond 2002). Kudoh & Basu (2011) rely on (shock) compressions due to supersonic turbulence, leading to steep gradients and thus to a local acceleration of ambipolar diffusion in the shocked regions (see also Li & Nakamura 2004). Whether turbulent diffusion really wins over accretion to make the sheet supercritical probably is best tested with a simulation along the lines of Kudoh & Basu (2011), but adding mass to the (sheet-like) cloud.

4.2 Filaments

4.2.1 Choice of Length Scales

Figures 5 and 6 highlight the effect of setting a specific length scaley by mapping the shortest timescales in the (L, n)-plane. There are two characteristic scales now (for an infinite filament): the radial extent, here described by the scale radius

$$R_0^2 = \frac{2c_s^2}{\pi G \rho_c} \tag{23}$$

(Ostriker 1964), and the length scale of the gravitationally most unstable mode along the filament. Both are marked in the Figures by short-dashed and solid lines, respectively. The longitudinal timescale (*lon*, blue) refers to the global criticality (eq. 21) of a *finite* filament at a given length indicated by L (x-axis). Following Bastien's (1983) analysis, we assume that the filament must have an aspect ratio of > 2 for longitudinal collapse to be viable. Chosing a density n (y-axis) results in a filament scale radius R_0 (dashed line). Together with an assumed filament length, results for any aspect ratio can be read off. The longitudinal fragmentation timescale (*frg*, red) refers to the gravitationally most unstable mode (Nagasawa 1987) for an infinite filament.

The time evolution of a filament maps slightly differently to these plots, compared to the sheet case. There, the magnetic field strength does not change, whereas, here, $B \propto \rho^{1/2}$. To help understanding the time sequence, we overplotted the positions of the two models shown in Fig-

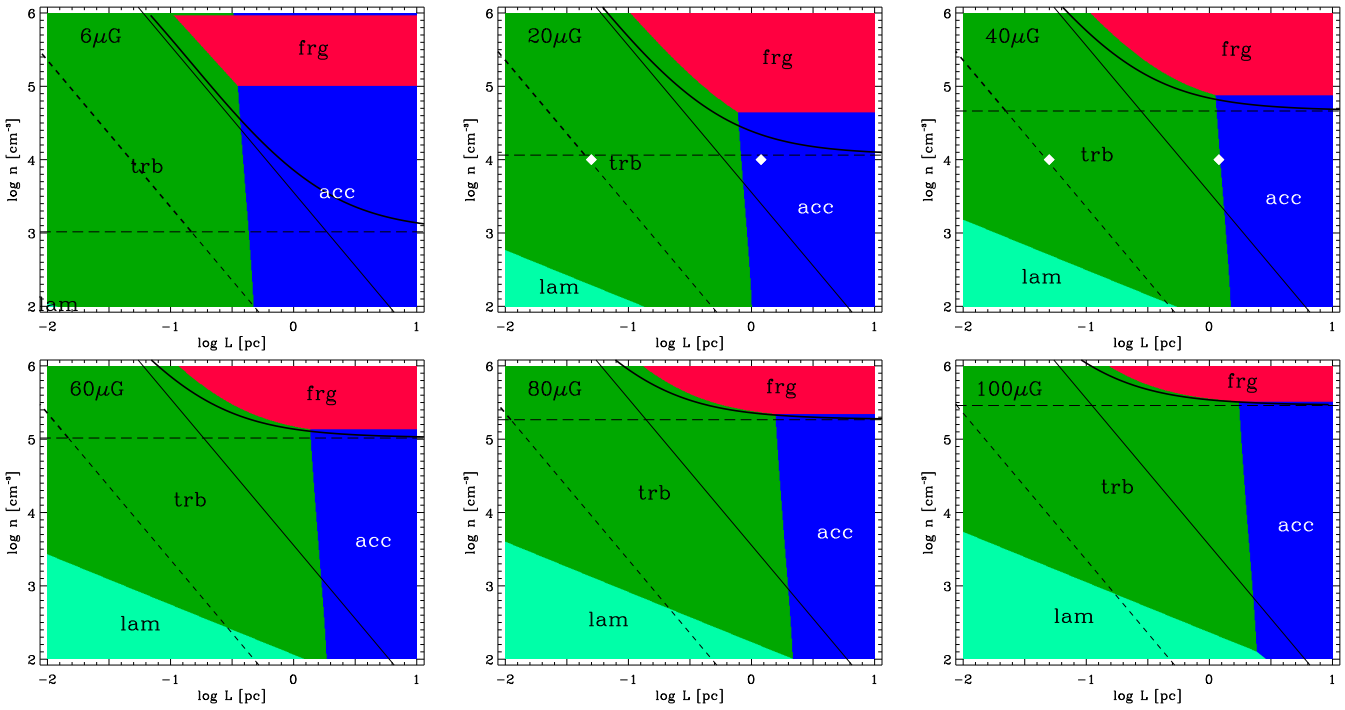

Figure 4. Same as Figure 3 including the turbulent diffusion timescale. Map of the shortest timescales in lengthscale-density plane, for a sheet. For a given combination of (L, n), all relevant timescales are compared, and the regime of the shortest timescale is color-coded as blue for accretion (*acc*), red for gravitational fragmentation (*frg*), light green for laminar ambipolar diffusion (*lam*), and dark green for turbulent diffusion (*trb*). The solid curved line shows the wavelength of the most unstable (magnetized) mode, λ_{max}, against the sheet's central density (Larson 1985), the solid straight line is the corresponding hydrodynamical mode, and the dashed line shows the sheet's scaleheight against central density. Criticality is indicated by the horizontal, long-dashed line (eq. 22). White diamonds show the initial conditions for models run by Kudoh & Basu (2011, see Sec.4.1.2).

ure 2 in (L, n)-space, for each magnetic fieldstrength. We use two characteristic scales, the most unstable mode (filled symbols), and the scale radius R_0 (eq. 23, open symbols), to highlight the role of the scale choice. We note two issues: (a) Evolving from weak to strong fields, all filaments (in the laminar case) on scales between 0.1 and 10 pc start out in a region where criticality is reached faster by accretion than by ambipolar diffusion, if we interpret R_0 and λ_{max} as a lower and upper bound for reasonable physical scales. Only at higher magnetic fields (later in the evolution), some of the models enter the ambipolar diffusion regime (*lam*, light green) on scales of R_0. Yet, at those densities, the filament is already radially and longitudinally supercritical (the densities reside above the long-dashed and dotted lines). (b) With increasing field strength, the lines for longitudinal and radial criticality (long dashed and dotted) move to higher densities, yet, if we interpret the sequence of magnetic fields as evolutionary sequence, we conclude that the filaments evolve faster to higher densities than the critical density with increasing field strength. *Taken together, these two observations show that even if the filament started out subcritical, it is driven to supercriticality by accretion rather than by laminar ambipolar diffusion.*

A fair fraction of the small scales is residing in the regime dominated by turbulent diffusion (Fig. 6, *trb*, dark green). Similarly as in the discussion of turbulent diffusion in sheets, it remains to be seen what the actual characteristic length scales are. Turbulent diffusion does not play a role on the scale of the most unstable mode, but it may play a role on scales a few times the core radius (few tenths of a parsec). Overall, with increasing field strength, the regime of turbulent diffusion dominance recedes to higher densities and smaller scales.

Another way to see this is that longitudinal collapse (fragmentation) dominates until the aspect ratio approaches 2, i.e. once the filament has evolved (fragmented) into a prestellar core. While formally we enter the turbulent diffusion regime at that point, it should be noted that for all practical purposes, the densities are well above the longitudinal and radial critical density, i.e. the structure is already supercritical and does not need any help from ambipolar diffusion.

5 SUMMARY

Our discussion of the dominant timescales in accreting, magnetized sheets and filaments is motivated by two observations. First, magnetic fields seem to be fairly well-ordered around filamentary molecular clouds (Alves et al. 2008; Palmeirim et al. 2013; Li et al. 2013), suggesting large-scale (accretion) flows along the field lines. Evidence for gas accretion onto filaments is mounting (Kirk et al. 2013; Friesen et al. 2013). Second, while the diffuse interstellar medium is generally magnetically subcritical, the dense gas ($n \gtrsim 300$ cm^{-3}) seems to be on average slightly supercritical by a factor of 2 (Crutcher et al. 2010). Two ideas have

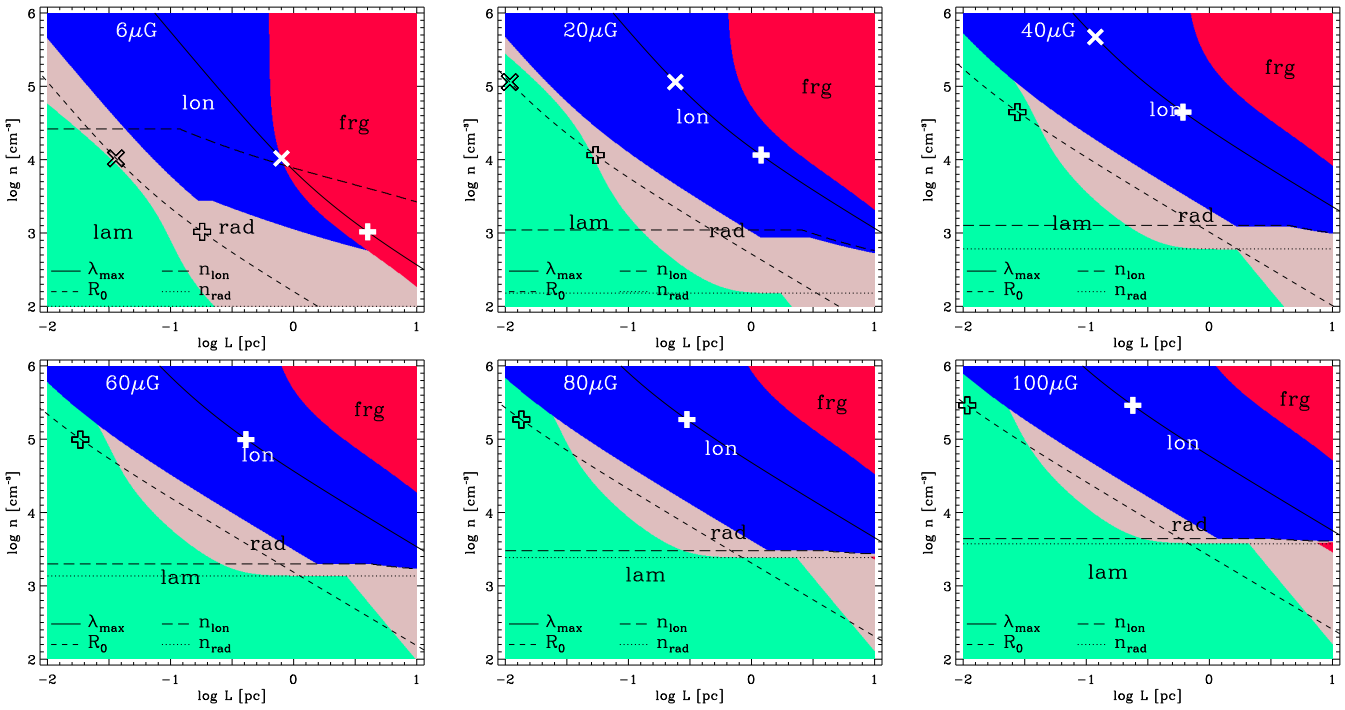

Figure 5. Map of the shortest timescales in the lengthscale-density plane, for a filament. For a given combination of (L, n), all relevant timescales are compared, and the regime is color-coded as longitudinal criticality (blue, *lon*), radial criticality (pink, *rad*), gravitational fragmentation (frg, *red*), and laminar ambipolar diffusion (light green, *lam*). The solid line shows the wavelength of the most unstable mode, λ_{max} (Nagasawa 1987) against the filament density, and the dashed line shows the filament's core-radius R_0 (eq. 23). Longitudinal criticality is indicated by the long-dashed line (eq. 21), and radial criticality by the dotted line. Symbols denote the evolution of the two filament accretion models shown in Fig. 2.

been suggested for the transition between sub- and supercriticality: ambipolar diffusion (based on Mestel & Spitzer 1956, more recently Kudoh & Basu 2008, 2011), and accretion (Vázquez-Semadeni et al. 1995; Hartmann et al. 2001). We explore the role of ambipolar diffusion and accretion to drive an initially subcritical sheet or filament to criticality, by comparing the relevant timescales.

(1) While ambipolar diffusion is present, it does not affect the evolution of an accreting sheet or filament. The accretion timescales are substantially shorter in the subcritical regime, rendering sheets (Fig. 3) and filaments (Fig. 5) supercritical before laminar ambipolar diffusion can affect the mass-to-flux ratio substantially. This agrees with the findings of Kudoh & Basu (2011), who quote timescales of a few 10^7 years to drive a sheet to criticality via laminar ambipolar diffusion. For sheets, increasing densities reduce the importance of laminar ambipolar diffusion, while for filaments, the ambipolar diffusion regime can be re-entered for high densities and small scales, yet at a stage when the filament has turned substantially supercritical.

(2) Turbulent diffusion may be important in a sheet-like geometry (Fig. 4) for strong magnetizations ($B > 20\mu$G). Yet, such a field strength would be a factor 2 to 4 higher than observed in the diffuse interstellar gas. In other words, the strong magnetizations refer to a stage of the cloud when the field has been amplified well beyond its background level – by gravity. For filaments (Fig. 6), turbulent diffusion plays only a role for small scales – and only, once the filament has been driven to criticality by accretion.

Note that we are *not* arguing that all regions of molecular clouds are magnetically supercritical. Rather, our analysis shows that the densest regions of such clouds wherein star formation takes place will generally become supercritical due to the accumulation of mass – that is, as a result of their formation – before ambipolar diffusion becomes important. Magnetic fields may still be important globally in reducing the efficiency of star formation. In fact Crutcher et al. (2010) point out that some clouds may well be magnetically dominated, and in any case the mean mass-to-flux ratio they infer in dense regions is only a factor of two above criticality, suggesting that magnetic forces do play a dynamical role (see Heitsch et al. 2001; Vázquez-Semadeni et al. 2005; Price & Bate 2008, for how supercritical magnetic fields affect the gravitational fragmentation and collapse). Marchwinski, Pavel, & Clemens (2012) demonstrate with infrared polarimetry mapping how strongly the mass-to-flux ratio can vary across a single cloud (see their Fig. 14).

We conclude that the effects of accretion must be considered in any analysis of the dynamical state of dense star-forming gas. We further find that laminar or turbulent diffusion – while present – is unlikely to control the evolution of a cloud from subcritical to supercritical.

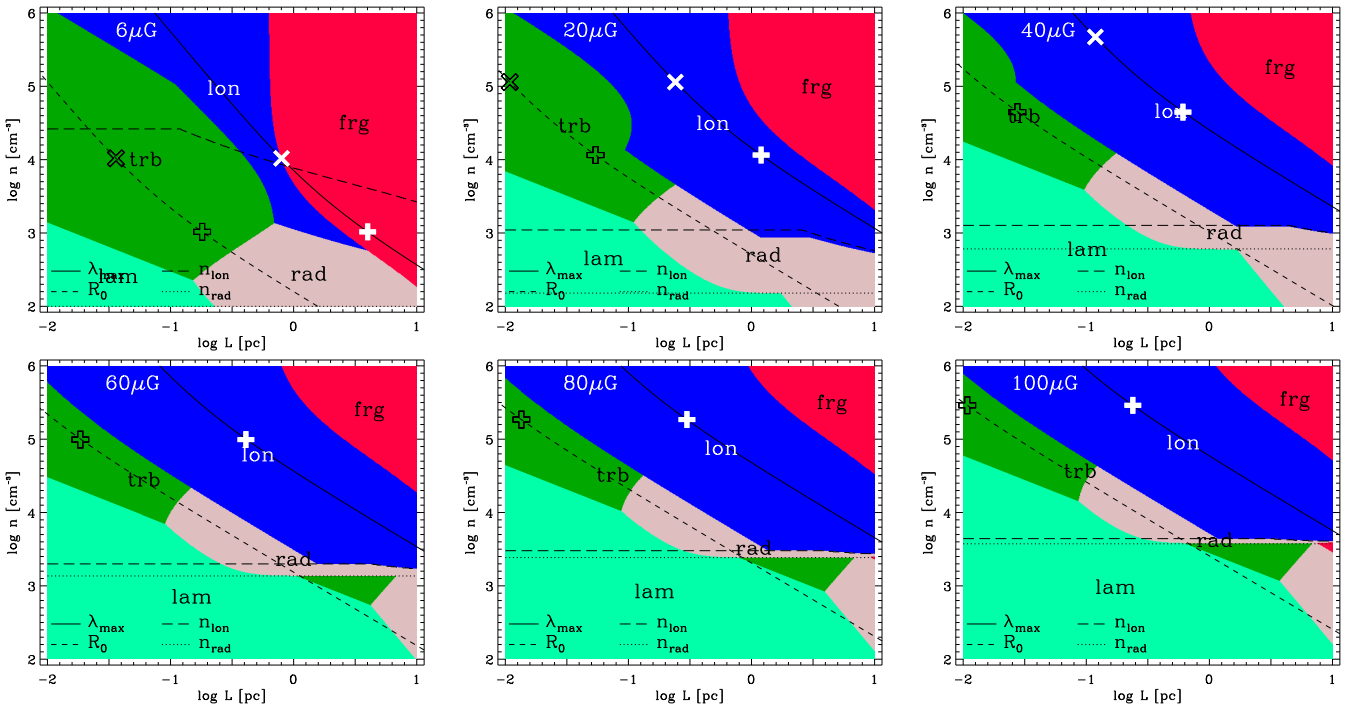

Figure 6. Same as Fig. 5, including turbulent diffusion. Map of the shortest timescales in the lengthscale-density plane, for a filament. For a given combination of (L, n), all relevant timescales are compared, and the regime is color-coded as longitudinal criticality (blue, *lon*), radial criticality (pink, *rad*), gravitational fragmentation (frg, *red*), laminar ambipolar diffusion (light green, *lam*), and turbulent (dark green, *trb*). The solid line shows the wavelength of the most unstable mode, λ_{max} (Nagasawa 1987) against the filament density, and the dashed line shows the filament's core-radius R_0 (eq. 23). Longitudinal criticality is indicated by the long-dashed line (eq. 21), and radial criticality by the dotted line. Symbols denote the evolution of the two filament accretion models shown in Fig. 2.

ACKNOWLEDGEMENTS

We thank the referee for a thought-provoking report. FH acknowledges support by UNC-CH. LH acknowledges partial support by UM.

APPENDIX A: AMBIPOLAR DIFFUSION TIMESCALE

The ambipolar diffusion timescale over a length scale L at an ambipolar diffusivity λ_{AD} is given by

$$\tau_{AD} = \frac{L^2}{\lambda_{AD}}. \tag{A1}$$

Following Heitsch & Zweibel (2003), we write λ_{AD} in dependence of the field strength B, the ion and neutral particle densities n_i and n_n, and the molecular weights $\mu_i = 29$ and $\mu_n = 2$, assuming a single species of HCO^+ and H_2 each – the exact choices do not affect the results. For instance, choosing C^+ and H for diffuse clouds results in $\mu_i\mu_n/(\mu_i + \mu_n) = 0.92$ instead of 1.87. We also need the ionization fraction $x_i \equiv n_i/n_n$, and the rate coefficient for elastic collisions $\langle\sigma v\rangle = 1.5 \times^1 0{-}9$ cm^3 s^{-1} (Draine et al. 1983). Taken together, this results in

$$\lambda_{AD} = \frac{\mu_i + \mu_n}{4\pi\langle\sigma v\rangle\mu_i\mu_n m_H x_i}\left(\frac{B}{n_n}\right)^2. \tag{A2}$$

Assuming ionization-recombination balance, the ionization degree can be approximated by

$$x_i = 1.2 \times 10^{-5} n_n^{-1/2} \tag{A3}$$

(Elmegreen 1979; Umebayashi & Nakano 1980). Then the ambipolar diffusivity can be written (for molecular cloud conditions) as

$$\lambda_{AD} = 8.2 \times 10^{16} \left(\frac{B}{5\mu\mathrm{G}}\right)^2 \left(\frac{n}{300\ \mathrm{cm}^{-3}}\right)^{-3/2}\ \mathrm{cm}^2\mathrm{s}^{-1}, \tag{A4}$$

and the ambipolar diffusion timescale reads

$$\tau_{AD} = 1.38{\times}10^3 \left(\frac{L}{\mathrm{pc}}\right)^2 \left(\frac{n}{3\times10^2\mathrm{cm}^{-3}}\right)^{3/2} \left(\frac{B}{5\mu\mathrm{G}}\right)^{-2}\ \mathrm{Myr}. \tag{A5}$$

We note that equation A3 applies to conditions within dense molecular clouds, with cosmic rays as the only ionization source. Thus, equation A5 tends to *underestimate* the ionization degree for diffuse gas, specifically for conditions with $A_V < 1$. In other words, until the ambient UV field has been shielded, ambipolar diffusion will be irrelevant. From equation 2, we see that the shielding column density corresponds to a field strength of $\approx 8\mu$G.

APPENDIX B: NEGLECTING THE AMBIENT GAS COLUMN

Equation 7 is only valid if the column density does not change appreciably while a single column out to z_{ref} is be-

ing accreted, or if $\Sigma_{acc} \ll \Sigma$. If we assume that $z_{ref} \gg H$, the argument is simplified, while considering the most unfavorable case. The ambient column then can be written as

$$N_{acc} = \frac{\Sigma_{acc}}{\mu m_H} = 6.2 \times 10^{18} \left(\frac{z_{ref}}{\mathrm{pc}}\right) \left(\frac{n_0}{\mathrm{cm}^{-3}}\right) \ \mathrm{cm}^{-2}. \quad \text{(B1)}$$

The constant term b (eq. 12) in equation 13 corresponds to the equivalent column of an isothermal sheet of scale height z_{ref}, and can be written as

$$\frac{b}{\mu m_H} = 1.58 \times 10^{20} \left(\frac{c_s}{0.2 \ \mathrm{km \ s}^{-1}}\right) \left(\frac{z_{ref}}{\mathrm{pc}}\right)^{-1} \ \mathrm{cm}^{-2} \quad \text{(B2)}$$

for $\mu = 2.36$. Thus, N_{acc} is generally negligible.

APPENDIX C: NEGLECTING RAM PRESSURE OF INFLOWS

By setting the lower accretion bound to the scaleheight of the sheet, we assumed that the ram pressure of the infalling gas, $p_{ram} = \rho_0 v_z(H)^2$, can be neglected, and thus does not compress the sheet noticeably. We show this by comparing p_{ram} to the internal sheet pressure, $p_{int} = \pi G \Sigma/2$. Then,

$$\frac{p_{ram}}{p_{int}} = 2.5 \times 10^{-2} \left(\frac{n_0}{\mathrm{cm}^{-3}}\right) \left(\frac{z_{ref}}{\mathrm{pc}}\right) \left(\frac{N}{10^{21} \mathrm{cm}^{-2}}\right)^{-1}. \quad \text{(C1)}$$

Here, we have assumed that $H/z_{ref} \ll 1$, an assumption that actually increases p_{ram}. Thus, the above expression is a conservative estimate. It also should be noted that for all practical purposes, a compression of the sheet by a factor of 2 or so would not affect our results qualitatively, since, again, the case $H/z_{ref} \ll 1$ would be reached earlier, thus just simplifying the arguments presented above.

APPENDIX D: GRAVITATIONALLY UNSTABLE MODES IN SHEETS

The frequency and wavenumber for the gravitationally most unstable mode in an infinite, magnetized sheet were derived from equations 13, 29, and 30 given by Larson (1985). Specifically, we numerically found the maximum of the disperson relation $\Omega(\nu, \mu)$, and fit a 5th-order polynomial of the form

$$\Omega_{max}(\mu) = \sum_0^5 c_i \mu^i \quad \text{(D1)}$$

to the values $\Omega(\mu)$ and $\nu(\mu)$. Here, $\Omega = \imath\omega H/c_s$, and $\nu = kH$. The strength of the magnetic field is set by the magnetic criticality parameter

$$\mu = \frac{2\pi\sqrt{G}\Sigma}{B}. \quad \text{(D2)}$$

The actual coefficients are listed in Table D1. The fits are accurate to $< 2\%$ between $1.1 < \mu < 18$, and $< 10\%$ for $1.009 < \mu < 30.1$. Beyond those values of μ, the fits should not be used.

APPENDIX E: DIFFUSION DUE TO UNBENDING OF FIELDLINES

If horizontal compressions occur in an accreting sheet, the field lines will bend slightly. This leads to a restoring force on the order of $\sim B^2(1 + \tan\alpha)/(2\pi H)$, with $\tan\alpha \ll 1$ as the angle between the horizontal field perturbation and the vertical background field, and H the scale height of the sheet. The restoring force can lead to two effects. If the mass loading of the field lines is low (i.e. the inertia of the sheet is small), the field lines can straighten without diffusion, i.e. Σ/B is conserved. This would be essentially a magnetosonic wave in the sheet plane. If the mass loading is high, the field might unbend by diffusing horizontally through the sheet. The timescale would be $H^2 \tan^2\alpha/\lambda_{AD}$, i.e. equation A5 multiplied by $\tan^2\alpha$. For small angles, this could reduce the AD timescale substantially. However, for a one-dimensional, horizontal compression (assuming symmetry), Σ/B would increase only by a factor of $(1 + 2\tan\alpha)$, so that this mechanism would play a role only when $\mu \approx 1$ already. The situation of the sheet as discussed here is different from that in accretion disks (e.g. Lubow et al. 1994; Okuzumi et al. 2014), where a steady-state solution can be found between (radial) field advection and diffusion.

REFERENCES

Alves F. O., Franco G. A. P., Girart J. M., 2008, A&A, 486, L13

André P. et al., 2010, A&A, 518, L102

Ballesteros-Paredes J., Gómez G. C., Pichardo B., Vázquez-Semadeni E., 2009, MNRAS, 393, 1563

Ballesteros-Paredes J., Gómez G. C., Loinard L., Torres R. M., Pichardo B., 2009, MNRAS, 395, L81

Ballesteros-Paredes J., Hartmann L., 2007, Revista Mexicana de Astronomia y Astrofisica, 43, 123

Bastien P., 1983, A&A, 119, 109

Burkert A., Hartmann L., 2004, ApJ, 616, 288

Ciolek G. E., Basu S., 2000, ApJ, 529, 925

Ciolek G. E., Basu S., 2006, ApJ, 652, 442

Ciolek G. E., Mouschovias T. C., 1993, ApJ, 418, 774

Cohen M., Kuhi L. V., 1979, ApJL, 227, L105

Crutcher R. M., Wandelt B., Heiles C., Falgarone E., Troland T. H., 2010, ApJ, 725, 466

Dale J. E., Bonnell I. A., Clarke C. J., Bate M. R., 2005, MNRAS, 358, 291

Dale J. E., Ercolano B., Bonnell I. A., 2012, MNRAS, 424, 377

Draine B. T., Roberge W. G., Dalgarno A., 1983, ApJ, 264, 485

Elmegreen B. G., 1979, ApJ, 232, 729

Evans II N. J., et al., 2009, ApJS, 181, 321

Eyink G., Vishniac E., Lalescu C., Aluie H., Kanov K., Bürger K., Burns R., Meneveau C., Szalay A., 2013, Nature, 497, 466

Eyink G. L., Lazarian A., Vishniac E. T., 2011, ApJ, 743, 51

Fatuzzo M., Adams F. C., 2002, ApJ, 570, 210

Fischera J., Martin P. G., 2012a, A&A, 547, A86

Fischera J., Martin P. G., 2012b, A&A, 542, A77

Franco J., Shore S. N., Tenorio-Tagle G., 1994, ApJ, 436, 795

Table D1. Fits are limited to $1.009 < \mu < 30.1$.

	c_0	c_1	c_2	c_3	c_4	c_5
Ω_{max}	0.0027172332	−0.093767163	1.1779378	−1.1181161	0.38624833	−0.043026629
ν_{max}	0.0029897751	−0.089183578	1.0381798	−0.69517753	0.074091029	0.027382362

Friesen R. K., Medeiros L., Schnee S., Bourke T. L., Francesco J. D., Gutermuth R., Myers P. C., 2013, MNRAS, 436, 1513

Goodman A. A., Bastien P., Menard F., Myers P. C., 1990, ApJ, 359, 363

Hartmann L., 2002, ApJ, 578, 914

Hartmann L., Ballesteros-Paredes J., Bergin E. A., 2001, ApJ, 562, 852

Heiderman A., Evans II N. J., Allen L. E., Huard T., Heyer M., 2010, ApJ, 723, 1019

Heitsch F., 2013a, ApJ, 769, 115

Heitsch F., 2013b, ApJ, 776, 62

Heitsch F., Ballesteros-Paredes J., Hartmann L., 2009, ApJ, 704, 1735

Heitsch F., Hartmann L., 2008, ApJ, 689, 290

Heitsch F., Mac Low M.-M., Klessen R. S., 2001, ApJ, 547, 280

Heitsch F., Stone J. M., Hartmann L. W., 2009, ApJ, 695, 248

Heitsch F., Zweibel E. G., 2003, ApJ, 583, 229

Heitsch F., Zweibel E. G., Slyz A. D., Devriendt J. E. G., 2004, ApJ, 603, 165

Heyer M. H., Vrba F. J., Snell R. L., Schloerb F. P., Strom S. E., Goldsmith P. F., Strom K. M., 1987, ApJ, 321, 855

Inoue T., Inutsuka S.-i., 2008, ApJ, 687, 303

Inoue T., Inutsuka S.-i., 2009, ApJ, 704, 161

Kim E.-J., Diamond P. H., 2002, ApJL, 578, L113

Kim W.-T., Ostriker E. C., 2006, ApJ, 646, 213

Kirk H., Myers P. C., Bourke T. L., Gutermuth R. A., Hedden A., Wilson G. W., 2013, ApJ, 766, 115

Klessen R. S., Hennebelle P., 2010, A&A, 520, A17

Kudoh T., Basu S., 2008, ApJL, 679, L97

Kudoh T., Basu S., 2009, in Revista Mexicana de Astronomia y Astrofisica Conference Series Vol. 36 of Revista Mexicana de Astronomia y Astrofisica Conference Series, Molecular cloud fragmentation driven by gravity, ambipolar diffusion and nonlinear flows: three-dimensional simulations. p. 278

Kudoh T., Basu S., 2011, ApJ, 728, 123

Lada C. J., Lombardi M., Alves J. F., 2010, ApJ, 724, 687

Larson R. B., 1985, MNRAS, 214, 379

Lazarian A., Vishniac E. T., 1999, ApJ, 517, 700

Li H.-B., Fang M., Henning T., Kainulainen J., 2013, MNRAS, 436, 3707

Li Z.-Y., Nakamura F., 2004, ApJL, 609, L83

Lubow S. H., Papaloizou J. C. B., Pringle J. E., 1994, MNRAS, 267, 235

Marchwinski R. C., Pavel M. D., Clemens D. P., 2012, ApJ, 755, 130

Mestel L., Spitzer Jr. L., 1956, MNRAS, 116, 503

Moneti A., Pipher J. L., Helfer H. L., McMillan R. S., Perry M. L., 1984, ApJ, 282, 508

Mouschovias T. C., 1979a, ApJ, 228, 475

Mouschovias T. C., 1979b, ApJ, 228, 159

Nagasawa M., 1987, Progress of Theoretical Physics, 77, 635

Nakano T., Nakamura T., 1978, PASJ, 30, 671

Okuzumi S., Takeuchi T., Muto T., 2014, ApJ, 785, 127

Ostriker J., 1964, ApJ, 140, 1056

Palmeirim P., et al., A&A, 550, A38

Pety J., et al., 2013, ApJ, 779, 43

Pon A., Toalá J. A., Johnstone D., Vázquez-Semadeni E., Heitsch F., Gómez G. C., 2012, ApJ, 756, 145

Price D. J., Bate M. R., 2008, MNRAS, 385, 1820

Santos-Lima R., Lazarian A., de Gouveia Dal Pino E. M., Cho J., 2010, ApJ, 714, 442

Shu F. H., Adams F. C., Lizano S., 1987, ARAA, 25, 23

Tomisaka K., 2013, in Protostars and Planets VI, Heidelberg, July 15-20, 2013. Poster #1S026 Structure and Mass of Filamentary Isothermal Cloud Threaded by Lateral Magnetic Field. p. 26

Troland T. H., Heiles C., 1986, ApJ, 301, 339

Umebayashi T., Nakano T., 1980, PASJ, 32, 405

Vázquez-Semadeni E., Colín P., Gómez G. C., Ballesteros-Paredes J., Watson A. W., 2010, ApJ, 715, 1302

Vázquez-Semadeni E., Gómez G. C., Jappsen A. K., Ballesteros-Paredes J., González R. F., Klessen R. S., 2007, ApJ, 657, 870

Vázquez-Semadeni E., Kim J., Ballesteros-Paredes J., 2005, ApJL, 630, L49

Vázquez-Semadeni E., Passot T., Pouquet A., 1995, ApJ, 441, 702

Walch S. K., Whitworth A. P., Bisbas T., Wünsch R., Hubber D., 2012, MNRAS, 427, 625

Zweibel E. G., 2002, ApJ, 567, 962